A: Kinetics, Dynamics, Photochemistry, and Excited States

n # #* Interactions in N-Acyl Homoserine Lactone (AHL) Derivatives and Their Effects on Hydrolysis Rates

Daniel J. Schmucker, Sydney R. Dunbar, Tricia D. Shepherd, and Michael A. Bertucci

J. Phys. Chem. A, **Just Accepted Manuscript** • DOI: 10.1021/acs.jpca.8b12266 • Publication Date (Web): 11 Mar 2019

n → π* Interactions in N-Acyl Homoserine Lactone (AHL) Derivatives and Their Effects on Hydrolysis Rates

Daniel J. Schmucker[†], Sydney R. Dunbar[‡], Tricia D. Shepherd[†], and Michael A. Bertucci[*†]

[†]*Department of Chemistry, Moravian College, 1200 Main St., Bethlehem, PA 18018*

[‡]*Department of Chemistry, Hartwick College, 1 Hartwick Dr., Oneonta, NY 13820*

Abstract:

N-acyl homoserine lactones (AHLs) mediate population-wide behavioral changes in gram-negative bacteria through quorum sensing (QS), a process shown to regulate virulence, biofilm formation, and other phenotypes that impact human health. AHLs have been proposed to contain an n → π* interaction that reduces the molecules' susceptibility to signal inactivation via lactone hydrolysis. In this work, seven AHL derivatives were modeled via gas-phase DFT calculations, implicit solvent DFT calculations, and MD simulations. Each derivative was then synthesized and hydrolyzed to probe the relationship between the strength of the orbital interaction and hydrolysis rate. The data obtained support that an increase in n → π* energy ($E_{n\rightarrow\pi^*}$) correlates to a decrease in the hydrolysis rate constant (k_{obs}). Further, the observed variation in these rates demonstrates that AHL hydrolysis can be modified by manipulating steric and electronic effects that alter the electrophilicity of the lactone carbonyl. These results help to elucidate nature's choice of AHLs as agents of density-dependent bacterial communication and could inform the design of AHL-based quorum sensing modulators.

Introduction:

With the emergence of virulent bacterial strains that have developed resistances to current treatments, as observed in opportunistic human pathogen *Pseudomonas aeruginosa*, efficacy of

traditional antibiotics is decreasing.[1] Thus, the discovery of new treatments is in high demand and the movement towards novel antimicrobial strategies has become more prominent.[2,3] One process that has been linked to bacterial virulence is quorum sensing (QS). QS is density-dependent chemical communication that permits unified gene expression amongst bacteria and results in such phenotypes as competence, the production of virulence factors, and biofilm formation.[4-7]

In gram-negative bacteria, such as *Pseudomonas aeruginosa*, QS processes rely on the self-production of signaling molecules known as *N*-Acyl-Homoserine Lactones (AHLs) for intercellular communication.[8,9] Amongst the variety present in different species of gram-negative bacteria, AHLs have been demonstrated to hydrolyze at variable rates.[10] This natural control of signal concentration allows the bacteria to accurately measure the population density in a given moment and regulate the initiation and duration of the multicellular event. When both the bacterial cell and unhydrolyzed AHL concentration are sufficiently high (Figure 1, **1**), the AHL binds to its cognate receptor and bacterial communication occurs. As the AHL is hydrolyzed (Figure 1, **2**) and the concentration of the active AHL decreases, the signal cannot bind and bacterial communication ceases.[10,11] This allows the QS mechanism to be controlled and gene expression to be "switched" on and off based on colony density. Hydrolytic enzymes (e.g. AHL lactonases) are produced by the quorate-forming bacteria to, in part, catalyze the silencing of QS

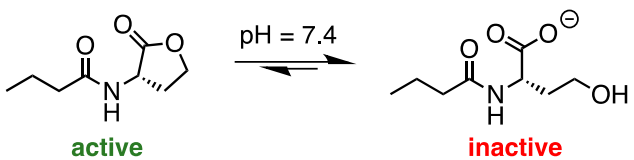

Figure 1. AHLs Undergo Hydrolysis. The reaction scheme above displays the hydrolysis of an AHL found in *P.aeruginosa* under physiological conditions. When the AHL is hydrolyzed, it is incapable of binding to its cognate receptor to stimulate gene expression.

signaling in this manner.[12,13] Thus, the stability of the lactone ring and its hydrolysis rate are critical for effective signaling. Controlling hydrolysis rates could be a strategy for designing AHL-like modulators to control gram-negative QS and manage its downstream effects, such as virulence factor production and biofilm formation.[14-17]

An n → π* interaction was recently proposed by Newberry and Raines between the lone pair of the amide O and the C=O π* orbital of the lactone of the AHL (Figure 2).[19] The presence of this orbital overlap was confirmed by a crystal structure of the unbound 3-oxobutanoyl AHL.[20] The n → π* interaction is a weak, attractive interaction that results from a sub-Van der Waals contact between a filled lone pair and a π antibonding orbital. This overlap has been implicated in protein folding and structure[21,22], RNA synthesis[23], and native chemical ligation.[24] In these systems, the donation of electron density to the π* orbital of the carbonyl has been demonstrated to reduce the electrophilicity of the C=O, increasing the energetic barrier for nucleophilic attack.[25]

Consequently, it has been hypothesized that the observed n → π* orbital overlap is responsible for slowing AHL hydrolysis in physiological environments, allowing the signal to persist during intercellular transport. If so, one should be able to develop AHL derivatives that enhance or reduce the strength of this key orbital overlap and observe a decrease or increase in AHL hydrolysis rates. In this work, a small library of AHL derivatives were computationally modeled, synthesized, and hydrolyzed to evaluate the correlation between n → π* orbital overlap and AHL hydrolysis rates. Verifying the impact of the n → π* interaction on hydrolysis would support consideration of the through-space interaction in the design of novel AHL derivatives for QS modulation.

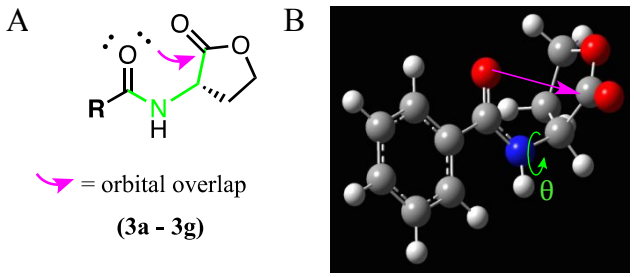

Figure 2. A Key Orbital Overlap in AHLs. (A) The described n → π* interaction occurs between the lone pair of the AHL amide oxygen and the π* antibonding orbital of the lactone carbonyl (pink arrow). The dihedral angle for C'_{i-1}–N_i–C^{α}_i–C'_i (θ, green) was measured to confirm the viability of an orbital overlap based on the lowest energy conformation. The library of AHL derivatives (**3a-3g**) in this study was modeled and synthesized with various aromatic substituents defined in Table 1. (B) Energy minimized structure of the phenyl substituted AHL with the n → π* overlap and measured dihedral angle θ indicated.

Experimental Methods:

DFT Calculations. All quantum mechanical calculations were performed by the Gaussian09 package.[26] Gas phase and implicit water (PCM[27]) optimizations were performed at the B3LYP\6-311+G(2d,p) and RB3LYP\6-31++G(d,p) levels of theory, respectively. The energies of the resultant structures were corrected by the zero-point vibrational energy and the optimized structures yielded no imaginary frequencies. In order to obtain values for the contribution of n→π* overlap, NBO analysis of the optimized conformations was completed at the same level of theory.[28]

MD Simulations. The general Amber force field (GAFF)[29] was used for MD simulations. Partial atomic changes were calculated at the HF-6.31G* level following the RESP[30] protocol as implemented in the antechamber module of the AmberTools18[31] package. All MD simulations were performed using AMBER 12 under periodic boundary conditions with 2 fs integration time. A single solute molecule was surrounded by a 10 Å box of TIP3P[32] water. After minimization (the steepest descent method for 2000 steps) and equilibration in NVT and NPT ensembles (for 20 and 60 ps, respectively), the simulation was performed at 300 K and at 1 bar for 12 ns. All

bonds containing hydrogen atoms were constrained using the SHAKE algorithm. A 10 Å cutoff value was adopted for nonbonded interactions, and long-range electrostatic interactions were handled with the PME scheme. Langevin dynamics was used to control temperature with a collision frequency of 2 ps^{-1} and a pressure coupling with 1 ps time constant.

Synthesis of *N*-Acyl Homoserine Lactone (AHL) Derivatives. In a 250-mL round bottom flask, 0.364 g (2 mmol) of α-amino-γ-butyrolactone hydrobromide was dissolved in 60 mL of dichloromethane (DCM). A stir bar and 0.836 mL (6 mmol) of triethylamine were added. The solution was placed on ice and the corresponding benzoyl chloride (2 mmol) was added. After sitting on ice for 30 mins, the ice bath was removed and the reaction was allowed to run for 4 h. Thin-layer chromatography (TLC) was used to monitor reaction progression and completion. Upon completion, the solvent was evaporated under reduced pressure. The reaction mixture was redissolved in 60 mL of EtOAc and washed in a separatory funnel with 1 M of $NaHCO_3$ (2x), saturated KOH (2x), and saturated NaCl (2x). The organic layer was collected, dried over Na_2SO_4, and concentrated under reduced pressure.[33] The product was redissolved in 3 mL of EtOAc and a silica column was run using a 75:25 EtOAc:Hexane mobile phase. The pure fractions, as determined by TLC, were combined and concentrated. For the 3-NO_2 AHL (**3f**), further purification via recrystallization in ethanol was required to remove minor impurities. ^{1}H-NMR and ^{13}C-NMR spectra were obtained for each product.

Phenyl N-acyl homoserine lactone **3a:** Yield 44.7 mg (10.9%); δ_H (CDCl3, 200MHz) 2.31 (1H, p), 2.83 (1H, m), 4.25-4.49 (2H, t), 4.81-4.90 (1H, m), 7.28-7.45 (4H, m), 7.77-7.81 (2H, d); δ_c (CDCl3, 50MHz) 176.1, 167.7, 132.9, 132.0, 128.6, 127.2, 66.3, 49.5, 30.0; ESI-TOF-MS $[M+H]^+$ calc. 205.0739, found 205.0743 (Δ1.94 ppm)

2-methoxyphenyl N-acyl homoserine lactone **3b:** Yield 119 mg (25.4%); δ_H (CDCl3, 200MHz) 2.15- 2.32 (1H, p), 2.71-2.84 (1H, m), 3.85 (3H, s), 4.22-4.71 (3H, m), 6.8-6.85 (1H, d), 6.96-7.0 (1H, t), 7.22-7.38 (1H, t), 8.07-8.11 (1H, d) 8.54-8.56 (1H, s); δ_c (CDCl3, 50MHz) 175.7, 165.4, 157.6, 133.3, 131.9, 121.0, 119.9, 111.2, 66.1, 55.8, 49.4, 29.9; ESI-TOF-MS $[M+H]^+$ calc. 235.0845, found 235.0853 (Δ3.47 ppm)

3-methoxyphenyl N-acyl homoserine lactone **3c:** Yield 39 mg (8.3%); δ_H (CD3CN -d3, 200MHz) 2.41-2.61 (3H, m), 3.85 (1H, s), 4.30 (1H, m), 4.47 (1H, t), 4.72 (1H, q), 7.10-7.16 (1H, m), 7.38 – 7.49 (4H, m); δ_c (CD3CN-d3, 50MHz) 175.2, 166.5, 159.8, 135.1, 129.8, 119.2, 117.4, 112.2, 65.7, 55.1, 48.8, 28.1; ESI-TOF-MS $[M+H]^+$ calc. 235.0845, found 235.0852 (Δ3.26 ppm)

4-methoxyphenyl N-acyl homoserine lactone **3d:** Yield 46 mg (9.8%); δ_H (CH3CN, 200MHz) 2.41-2.60 (2H, m), 3.86 (3H, s), 4.32 (1H, m), 4.47 (1H, m), 4.71 (1H, m), 6.98-7.01 (2H, d), 7.38-7.41 (1H, s), 7.80 (2H, d); δ_c (CDCl3, 50MHz) 175.9, 167.3, 162.7, 129.0, 125.2, 113.9, 66.3, 55.4, 49.7, 30.7; ESI-TOF-MS $[M+H]^+$ calc. 235.0845, found 235.0855 (Δ4.51 ppm)

2-nitrophenyl N-acyl homoserine lactone **3e:** Yield 32 mg (6.5%); δ_H (CD3CN-d3, 200MHz) 2.37-2.51 (1H, m), 2.66 (1H, m), 4.24-4.38 (1H, m), 4.47 (1H, m), 4.62-4.77 (1H, m), 7.52-7.83 (4H, m), 8.04-8.06 (1H, d); δ_c (CD3CN-d3, 50MHz), 175.9, 167.5, 148.4, 134.9, 132.9, 132.4, 130.2, 125.7, 67.1, 50.3, 29.3; ESI-TOF-MS $[M+H]^+$ calc. 250.0590, found 250.0600 (Δ3.97 ppm)

3-nitrophenyl N-acyl homoserine lactone **3f:** Yield 141 mg (28.1%); δ_H (CD3CN-d3, 200MHz) 2.44 (1H, p), 2.57 (1H, m), 4.29 (1H, m), 4.47 (1H, td), 4.75 (1H, m), 7.72 (2H, t), 8.19 (1H, d), 8.37 (1H, d), 8.62 (1H, s); δ_c (CD3CN-d3, 50MHz), 176.2, 166.0, 149.6, 136.3,

134.6, 131.5, 127.6, 123.4, 67.1, 50.3, 29.3; ESI-TOF-MS $[M+H]^+$ calc. 250.0590, found 250.0595 (Δ2.17 ppm)

4-nitrophenyl N-acyl homoserine lactone **3g:** Yield 124 mg (24.7%); δ_H (acetone-d6, 200MHz) 2.39-2.86 (2H, m), 4.32-4.55 (2H, m), 4.96 (1H, m), 8.16 (2H, d), 8.36 (2H, d), 8.56 (1H, s); δ_c (acetone-d6, 50MHz), 175.7, 166.2, 151.0, 140.7, 129.9, 124.9, 66.6, 50.3, 29.7; ESI-TOF-MS $[M+H]^+$ calc. 250.0590, found 250.0591 (Δ0.64 ppm)

Hydrolysis Rates via HPLC. Standard samples were made in acetonitrile at concentrations of 2.0 mM, 1.0 mM, 0.25 mM, 0.0625 mM, and 0.0156 mM for each AHL derivative through serial dilution. The samples were utilized to generate a calibration curve for the absorbance of each AHL at wavelengths of 220 nm and 254 nm.

To monitor the hydrolysis of each AHL derivative, a 50 mM stock solution of each AHL was prepared in 0.4 mL DMSO. Before the first HPLC injection, 0.08 mL of 50 mM stock solution was diluted with PBS buffer to 4.0 mL to obtain a final AHL concentration of 1.0 mM. The solution was immediately transferred to an HPLC vial and injected into the HPLC in 25-minute intervals to monitor the hydrolysis of the AHL over time at 25°C. The hydrolysis of each AHL was repeated independently in triplicate and the rate constant obtained from each trial was averaged to yield the reported k_{obs} value (see Table S2). The product peak in the 3-MeO AHL (**3c**) trial was collected to verify the formation of the hydrolysis product by HR-MS ($[M+H]^+$ calc. 253.0950, found 253.0961).

Results & Discussion:

We sought to design a model system that would allow methodical evaluation of the influence of structural and electronic effects on the strength of the n → π* overlap. Seven

aromatic AHL derivatives were considered, paralleling recently discovered agonists and antagonists of QS in *P.aeruginosa* and other gram-negative bacteria.[34,35,36] Phenyl AHL derivatives are not representative of the tremendous variety of QS modulators that have been developed nor do they represent the most potent inhibitors; however, employing them as our model system permits the synthesis and systematic evaluation of the n → π* energy in regioisomers (i.e. – *ortho, meta, para*) with defined Hammett parameters. As inductive effects have already been indicated to influence the strength of the n → π* overlap, we reasoned that simply incorporating electronegative substituents iteratively distanced from the acyl moiety would lead to a systematic increase in the orbital interaction.[37,38] To assess the impact of both inductive and resonance effects, methoxy (-OMe) and nitro (-NO_2) groups were chosen as substituents due to differences in their corresponding Hammett parameters σ_p and σ_m (Table 1). For instance, *para* –OMe, which has been shown to behave as either donor or acceptor based on its orientation[39], provides a net electron-donating effect to an adjacent π-system (σ_p = -0.27); *para* –NO_2 is electron-withdrawing (σ_p = +0.78). Finally, the –OMe and –NO_2 groups have notably different contributions with regards to steric strain, with experimentally determined A-values for -OMe = 0.75 kcal/mol and -NO_2 = 1.13 kcal/mol.[40] Our library contains regioisomers in which steric strain is elevated, like the 2-MeO and 2-NO_2 derivatives, allowing us to determine the role steric effects play in disrupting the key orbital overlap.

Gas-phase DFT calculations were completed on each library member at the B3LYP\6-311+G(2d,p) level of theory to obtain optimized conformations for each derivative and affirm the presence of an n → π* interaction. The n → π* overlap in the lowest energy conformation was obtained using natural bond orbital (NBO) analysis. Across the library, $E_{n\rightarrow\pi^*}$ were obtained from 0.60 to 0.76 kcal/mol and, in the case of the *ortho* and *meta*-substituted AHLs, were

detected in more than one optimized conformational state. The variation in conformation originated from changes in the O=C-C=C dihedral angle between the amide and phenyl moieties and the resultant orientation of the -NO_2 or -OMe substituent (see Table S3). The obtained $E_{n\rightarrow\pi^*}$ values are in agreement with the magnitudes reported by Newberry and Raines for such orbital interactions in their *N*-trimethyl and *N*-tribromo AHL derivatives.[19] Likewise, the O_n---C=O_{π^*} distances and $C'_{i-1}-N_i-C^{\alpha}_i-C'_i$ dihedral angles served as reliable indicators of the n → π* interaction. The calculated $C'_{i-1}-N_i-C^{\alpha}_i-C'_i$ dihedral angles ranged from 54.8° to 60.5° holding the distance between the donor oxygen and the carbonyl carbon of the lactone between 2.93 and 2.99 angstroms, an acceptable proximity for the proposed van der Waals contact to occur. To test for the possible disruption of the torsional profiles under a different DFT functional, the calculations were re-run under dispersion-corrected conditions (Empirical Dispersion = GD3). The dihedral angles persisted without significant change (see Table S4).

Despite evidence of the interaction in the gas-phase, the impact of the n → π* overlap on AHL confirmation in the presence of explicit solvent molecules has not been explored. Consequently, classical molecular dynamics (MD) simulations of each derivative in a box of water were performed to test the interaction's influence and resilience in this medium. All seven of the AHL derivatives adopted and held conformational states indicative of n → π* orbital overlap for varying lengths of time (see Supporting Information). These states were not the dominant conformations during the MD simulation, indicating that intermolecular forces from explicit solvent will compete with the n → π* overlap in solution. A selection of frames containing conformations that appeared to demonstrate the desired through-space interaction were analyzed. The characteristic O_n---C=O_{π^*} distances and $C'_{i-1}-N_i-C^{\alpha}_i-C'_i$ dihedral angles observed in the gas-phase and solvation DFT calculations were detected. Further, subsequent

snapshot quantum calculations revealed $E_{n\rightarrow\pi^*}$ values, validating the presence of through-space interaction.

Table 1: Implicit solvent energy-minimized conformational data for AHL derivatives

AHL	R	σ^a	θ (degrees)^b	d (angstroms)	θ_p (degrees)^c	$E_{n\rightarrow\pi^*}$ (kcal/mol)
3a	Ph	0.0	53.8	2.90	25.4	1.11
			53.9	2.89	-27.5	0.99
3b	2-MeOPh	-	53.8	2.86	180	1.20
			53.2	2.85	58.4	1.14
			54.5	2.92	-56.6	1.01
			54.2	2.91	-48.6	0.96
			53.8	2.93	59.1	0.86
3c	3-MeOPh	0.12	53.8	2.89	150	1.10
			53.8	2.89	-27	1.08
3d	4-MeOPh	-0.27	54.0	2.91	-21.1	1.12
			54.6	2.91	-23.1	1.09
3e	2-NO_2Ph	-	54.4	2.89	-54.9	1.15
			55.3	2.94	64.6	0.88
			56.4	2.97	-54.0	0.84
3f	3-NO_2Ph	0.71	53.9	2.90	-27.5	1.02
			54.1	2.91	26.7	0.93
3g	4-NO_2Ph	0.78	53.9	2.91	-30.3	0.98

[a]Values obtained from reference 41; [b]θ represents the C'_{i-1}–N_i–C^{α}_i–C'_i dihedral angle; [c]θ_p represents the (O=C-C=C) amide-phenyl dihedral angle

With support for the through-space interaction in a dynamic solvent environment, we sought to obtain $E_{n\rightarrow\pi^*}$ values that more closely described the AHL derivatives in water. The coordinates of the n → π*-containing conformations identified in the MD simulations were employed as the initial conformations for optimization calculations under implicit solvent conditions. Energy values corresponding to the predicted O_n---C=O_{π^*} orbital overlap were again detected in at least two different conformational states for each of the AHL derivatives, except the 4-NO_2 AHL, which only yielded one minimum (Table 1). These $E_{n\rightarrow\pi^*}$ values were larger than the gas-phase values, supported by the observed decrease in O_n---C=O_{π^*} distances and C'_{i-1}–N_i–C^{α}_i–C'_i dihedral angles. Importantly, the average increase was consistent across all seven of the AHL analogs. As we hypothesized, the proximity of the -NO_2 and -OMe groups to

the *N*-acyl moiety influenced the $E_{n\rightarrow\pi^*}$. The *ortho*-substituted derivatives (compounds **3b** and **3e**) displayed the largest number of conformations containing the n → π* interaction. They had the largest range of $C'_{i-1}-N_i-C^{\alpha}_i-C'_i$ dihedral angles and O_{i-1}---$C'_i=O_i$ distances, and consequently the greatest variety of $E_{n\rightarrow\pi^*}$ values. Thus, the influence of sterics is evident as it had an observable effect on the magnitude of the n → π* interaction. The results for the remaining AHL derivatives reveal the significant, differential impact the methoxy and nitro groups have on the orbital interaction. They displayed $E_{n\rightarrow\pi^*}$ values that moderately correlated to the known sigma values for each substituent and conformations that allow conjugation of the aryl ring and the adjacent carbonyl. If the largest observed $E_{n\rightarrow\pi^*}$ is considered, compound **3d** (4-MeO) has the strongest orbital overlap; it is the only member of the library that has a negative, or net electron-donating, Hammett parameter. Next in sequence is the phenyl AHL **3a**, with an $E_{n\rightarrow\pi^*}$ = 1.11 kcal/mol, followed by the net electron-withdrawing methoxy and nitro regioisomers, **3c, 3f,** and **3g**.

With computational evidence of the n → π* interaction and its magnitude in each derivative, we sought to experimentally determine its relationship to AHL hydrolysis. The seven AHL derivatives were synthesized by combining α-amino-γ-butyrolactone with a functionalized benzoyl chloride in the presence of base to establish the characteristic *N*-acyl bond (see Experimental Section). To simulate an extracellular physiological environment, PBS at pH = 7.4 was employed as the hydrolytic media. Each AHL was then dissolved in the buffer to an initial concentration of 1.0 mM and the resultant solution was injected at timed intervals into a RP-HPLC. Peaks corresponding to the AHL and the hydrolysis product were both monitored over time and, through a standard curve, the concentration of the AHL at each time point was determined (Figure 3). By fitting the acquired data, we confirmed that the hydrolysis proceeds

under pseudo-first order conditions and identified k_{obs} values for the hydrolysis of each AHL derivative (see Supporting Information).

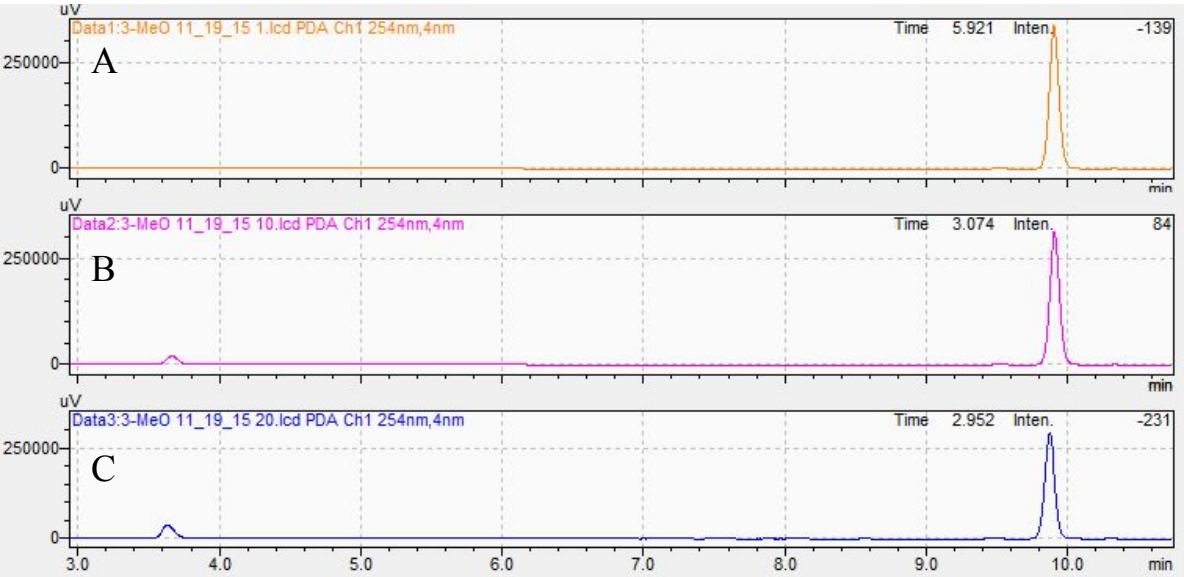

Figure 3. Monitoring AHL Hydrolysis**.** Hydrolysis of each AHL derivative was monitored overtime by RP-HPLC. The peaks with a retention time of 3.6 and 9.9 min correspond to the hydrolyzed and unhydrolyzed forms of the 3-MeO AHL (**3c**), respectively at (A) 7 min, (B) 232 min, and (C) 482 min.

The results displayed substantial differences in the hydrolysis rate constants of the AHL derivatives (Table 2). With reaction conditions remaining constant across all trials (i.e. temperature, pH, etc), only intrinsic properties should impact the hydrolysis rate constant. As the lactone itself is too many atoms removed from the substituent to influence hydrolysis in a through-bond manner, the variation in rate constant is evidence of a through-space effect, such as

Table 2. Rate constants for hydrolysis of AHL derivatives

Compound	R	k_{obs}[a](min^{-1})	Compound	R	k_{obs}[a](min^{-1})
3a	Ph	0.236	**3e**	2-NO_2Ph	0.345
3b	2-MeOPh	0.354	**3f**	3-NO_2Ph	0.318
3c	3-MeOPh	0.250	**3g**	4-NO_2Ph	0.381
3d	4-MeOPh	0.224			

[a]All k_{obs} values shown are equal to the number displayed x10^{-3} min^{-1}. Hydrolysis of each AHL derivative was completed in triplicate.

the n → π* interaction. The only AHL derivative with a larger $E_{n\rightarrow\pi^*}$ than the phenyl AHL (**3a**) is compound **3d**. The results of our kinetics experiments demonstrate that **3d** has the smallest rate constant, supporting the hypothesis that the n → π* interaction reduces the electrophilicity of the lactone. The k_{obs} values for the –OMe substituted AHLs decrease from compound **3c** to **3d**. This parallels the computed increase in the $E_{n\rightarrow\pi^*}$ as the methoxy group is moved further from the *N*-acyl lactone. Likewise, the NO_2-functionalized AHLs **3f** and **3g** with weaker n→π* energies hydrolyzed faster. Notably, compound **3g** was more susceptible to hydrolysis than **3b** and **3e**, despite the influence of steric effects that led to significant variability in calculated $E_{n\rightarrow\pi^*}$ values for **3b** and **3e**. However, the large positive σ_p value of **3g** supports the derivative as being the most electron-withdrawing regioisomer or the regioisomer that provides the least electron density to $\pi^*_{C=O}$. Thus, the stability of a single conformation in **3g** may amplify the impact of the -NO_2 electronic effects in enhancing the electrophilicity of the lactone C=O.

With more than one optimized confirmation identified for six of the AHL derivatives under implicit solvent conditions, the contribution of each to the observed hydrolysis rate is uncertain. However, for AHL analogs with two such conformations, it was observed that one of the $E_{n\rightarrow\pi^*}$ values almost perfectly aligned with the obtained hydrolysis rate. The result is a clear progression from increased $E_{n\rightarrow\pi^*}$ and reduced k_{obs} to decreased $E_{n\rightarrow\pi^*}$ and enhanced k_{obs} for the phenyl, *meta*-substituted *and para*-substituted AHLs (Table 3). Thus, a direct correlation is present between the implicit $E_{n\rightarrow\pi^*}$ values and hydrolysis rate. In addition, as the $E_{n\rightarrow\pi^*}$ of

Table 3. Implicit solvent data for lowest energy conformations of AHL derivatives

R	θ (degrees)	d (angstroms)	$E_{n\rightarrow\pi^*}$ (kcal/mol)	k_{obs} (min^{-1})
4-MeOPh	54.0	2.89	1.12	0.224
Ph	53.9	2.89	1.11	0.236
3-MeOPh	53.9	2.89	1.10	0.250
3-NO_2Ph	53.9	2.90	1.02	0.318
4-NO_2Ph	53.9	2.91	0.98	0.381

specific confirmations correlated most strongly to the observed hydrolysis rates, it can be inferred those conformations may be the dominant n → π* confirmations in solution. We refrained from selecting a single $E_{n\rightarrow\pi^*}$ for the *ortho*-substituted derivatives due to the increased number of optimized structures identified.

The magnitude of the rate constants obtained must also be noted. The hydrolysis rates of the library as a whole were quite slow, with the fastest derivative (**3g**) reaching only 6.1 – 7.9% completion after 3 hours. Nature's selection of AHLs as the key messenger for QS is at first perplexing as γ-butyrolactone alone has been shown to be resistant to hydrolysis at neutral pH.[42] This would be detrimental to a dynamic system like QS that requires timely activation and termination of colony-wide gene expression. On the other hand, the presence of an α-amino group substantially increases hydrolysis of the γ-butyrolactone (34% conversion in 4.25 h, Figure S1) due to inductive effects. AHLs are a unique class that are resistant to rapid hydrolysis, supporting the intercellular function of AHLs. Yet, AHLs are reactive enough to allow progressive silencing of the QS event they regulate, even in the absence of hydrolytic enzymes like AHL lactonases and acylases, that have been shown to mediate signal termination.[10,11,13] Our data supports the conclusion that the source of this balance is in part due to the n→π* interaction.

Through independent work published in 2011, Mattmann and colleagues screened **3d** and **3g** in *E.coli* reporter strains harboring QscR and LasR expression vectors to assess the agonism and antagonism of those AHL analogues at each receptor site. The 4-MeO substituted **3d** displayed 62% inhibition at QscR and 11% inhibition at LasR while in the presence of the native ligand. The 4-NO_2 substituted **3g** displayed 52% inhibition and 4 % inhibition at QscR and LasR, respectively.[29] These modest differences in inhibitory potency between the AHL derivatives correlate with our results. However, it is difficult to determine the impact of AHL

hydrolysis in this comparison. The assay completed by Mattmann et al. was only run for 4 - 6 hours, a timeframe in which the impact of signal degradation would only be 6.7 – 11.4% complete based on our observed rates for these AHL derivatives. In addition, previous work has identified a re-orientation of the AHL $C'_{i-1}-N_i-C^{\alpha}_i-C'_i$ dihedral angle and breaking of the n→π* interaction that occurs upon receptor binding. Our MD data shows that interconversion between conformations containing and not containing the n→π* interaction is common in explicit solvent, but aligning differences in $E_{n\rightarrow\pi^*}$ with differences target binding affinity would require further modeling and experimentation.[19]

Strengthening the n→π* interaction could provide a different advantage. This added stability may positively impact the pharmacokinetic profile of synthetic analogs designed for prophylaxis or infection treatment, a noted setback towards developing QS therapeutics.[43] In addition, strengthening the n→π* interaction allows the native lactone moiety to be preserved while minimizing QS inactivation by hydrolysis. This may preserve key AHL-receptor interactions as opposed to replacing the lactone with a non-hydrolyzable functionality. Thus, manipulating the strength of the orbital overlap to increase the lifetime of the unhydrolyzed form while maintaining the optimal conformational flexibility and connectivity for binding may aid in developing more potent QS modulators.

Conclusions:

Our acquired computational data combined with our experimental results strongly support the presence of an n→π* interaction in AHLs in a dynamic, solvated environment, and demonstrate the variability of the interaction's magnitude based on the functionalization of the *N*-acyl moiety. By modeling a series of AHL derivatives in accordance with defined Hammett

parameters, $E_{n\rightarrow\pi^*}$ values were obtained in both gas-phase and solvation models display the impact of electronic and steric effects on the donation of the oxygen lone pair to the lactone carbonyl. These energy values correlated with the derivatives' hydrolysis rates at pH = 7.4 for selected conformations. Obtained k_{obs} values varied from 0.224×10^{-3} to 0.381×10^{-3} min^{-1}, even within our small seven-membered model system. Thus, we have demonstrated that hydrolysis rate will vary depending on the functionalities incorporated into AHL derivatives, in part due to through-space orbital interactions. Consideration of these interactions (i.e. - $n\rightarrow\pi^*$) in the design of QS inhibitors may enhance their longevity in physiological environments, but they must remain weak enough to permit conformational modification for binding. We believe that evidence of this relationship will help inform those seeking to develop viable QS inhibitors for combating bacterial infectivity and resistance formation.

Supporting Information:

Procedures for synthesis of the AHL derivatives as well as data regarding kinetics experiments, HR-MS, NMR, MD and DFT calculations. This information is available free of charge via the Internet at http://pubs.acs.org.

Author Information:

Corresponding author: bertuccim@moravian.edu

Acknowledgements:

We would like to express our appreciation to Prof. Carl Salter at Moravian College and Prof. John Dudek at Hartwick College for helpful conversations as well as the department of chemistry

at University of Nevada, Reno for use of the TOF LC/MS spectrometer to acquire HR-MS data. This research was financially supported by departmental and start-up funds at Hartwick and Moravian College. Computational resources were provided in part by the MERCURY consortium (http://mercuryconsortium.org/) under NSF grants CHE-1229354 and CHE-1662030.

References:

(1) Mukherjee, S.; Moustafa, D.; Smith, C. D.; Goldberg, J. B.; Bassler, B. L. The RhlR quorum-sensing receptor controls *Pseudomonas aeruginosa* pathogenesis and biofilm development independently of its canonical homoserine lactone autoinducer. *PLOS Pathog.* **2017**, *13(7)*, e1006504.

(2) Rutherford, S. T.; Bassler, B. L. Bacterial quorum sensing: Its role in virulence and possibilities for its control. *Cold Spring Harb. Perspect. Med.* **2012**, *2*: a012427.

(3) Njoroge, J.; Sperandio, V. Jamming bacterial communication: New approaches for the treatment of infectious diseases: Quorum sensing inhibitors. *EMBO Mol. Med.* **2009**, *1*, 201–210.

(4) Waters, C. M.; Bassler, B. L. Quorum Sensing: Cell-to-cell communication in bacteria. *Annu. Rev. Cell Dev. Biol.* **2005**, *21*, 319–346.

(5) Olson, M. E. *et al.* Staphylococcus epidermidis agr quorum-sensing system: Signal identification, cross talk, and importance in colonization. *J. Bacteriol.* **2014**, *196*, 3482–3493.

(6) Yang, T.; Tal-Gan, Y.; Paharik, A. E.; Horswill, A. R.; Blackwell, H. E. Structure–function analyses of a *Staphylococcus epidermidis* autoinducing peptide reveals motifs critical for agrC-type receptor modulation. *ACS Chem. Biol.* **2016**, *11*, 1982–1991.

(7) Yang, Y,; Koirala, B.; Sanchez, L. A.; Phillips, N. R.; Hamry, S. R.; Tal-Gan, Y. Structure–activity relationships of the competence stimulating peptides (CSPs) in *Streptococcus pneumoniae* reveal motifs critical for intra-group and cross-group ComD receptor activation. *ACS Chem Biol.* **2017**, *12*, 1141–1151.

(8) Fuqua, C.; Greenberg, E. P. Signalling: Listening in on bacteria: acyl-homoserine lactone signaling. *Nat. Rev. Mol. Cell Biol.* **2002,** *3,* 685–695.

(9) Chhabra, S.; Philipp, B.; Eberl, L.; Givskov, M.; Williams, P.; Cámara, M. Extracellular Communication in Bacteria. *Top. Curr. Chem.* **2005,** *240,* 279–315.

(10) Yates, E. A.; Philipp, B.; Buckley, C.; Atkinson, S.; Chhabra, S. R.; Sockett, R. E.; Goldner, M.; Dessaux, Y.; Cámara, M.; Smith, H.; Williams, P. N-acylhomoserine lactones undergo lactonolysis in a pH-, temperature-, and acyl chain length-dependent manner during growth of *Yersinia pseudotuberculosis* and *Pseudomonas aeruginosa*. *Infect Immun,* **2002**, *70,* 5635–5646.

(11) Kaufmann, G. F.; Sartorio, R.; Lee, S.H.; Rogers, C. J.; Meijler, M. M.; Moss, J. A.; Clapham, B.; Brogan, A. P.; Dickerson, T. J.; Janda, K. D. Revisiting quorum sensing: Discovery of additional chemical and biological functions for 3-oxo-N-acylhomoserine lactones. *Proc Natl Acad Sci*, **2005**, *102,* 309–314.

(12) Wang, L. H.; Weng, L. X.; Dong, Y. H.; Zhang, L. H. Specificity and enzyme kinetics of the quorum-quenching *N*-acyl homoserine lactone lactonase (AHL-lactonase). *J. Biol. Chem.* **2004**, *279*, 13645-13651.

(13) Sio, C. F.; Otten, L. G.; Cool, R. H; Diggle, S. P.; Braun, P. G.; Bos, R.; Daykin, M.; Cámara, M.; Williams, P.; Quax, W. J. Quorum quenching by an *N*-acyl-homoserine lactone acylase from *Pseudomonas aeruginosa* PAO1. *Infect Immun* **2006**, *74*, 1673-1682.

(14) De Lamo Marin, S.; Xu, Y.; Meijler, M. M.; Janda, K. D. Antibody catalyzed hydrolysis of a quorum sensing signal found in Gram-negative bacteria. *Bioorg. Med. Chem. Lett.* **2007**, *17,* 1549–1552.

(15) Kaufmann, G. F.; Sartorio, R.; Lee, S.; Mee, J. M.; Altobell, L. J.; Kujawa, D. P.; Jefferies, E.; Clapham, B.; Meijler, M. M.; Janda, K. D. Antibody interference with *N*-acyl homoserine lactone-mediated bacterial quorum sensing. *J. Am. Chem. Soc.* **2006**, *128,* 2802–2803.

(16) Bertucci, M. A.; Lee, S. J.; Gagné, M. R. Thiourea-catalyzed aminolysis of N-acyl homoserine lactones. *Chem. Commun. 49,* **2013**, 2055-2057.

(17) Bertucci, M. A.; Lee, S. J.; Gagné, M. R; Selective transamidation of 3-oxo-N-acyl homoserine lactones by hydrazine derivatives. *Org. Biomol. Chem.* **2014**, *12,* 7197–7200.

(18) Chugani, S. A.; Whiteley, M.; Lee, K. M.; D'Argenio, D.; Manoil, C.; Greenberg, E. P. QscR, a modulator of quorum-sensing signal synthesis and virulence in Pseudomonas aeruginosa. *Proc Natl Acad Sci,* **2001**, *98,* 2752–2757.

(19) Newberry, R. W.; Raines, R. T. A key $n \rightarrow \pi^*$ interaction in *N*-acyl homoserine lactones. *ACS Chem. Biol.* **2014**, *9,* 880–883.

(20) Newberry, R. W.; Raines, R. T. Crystal structure of *N* -(3-oxobutanoyl)-L-homoserine lactone. *Acta Cryst. E,* **2016**, *72,* 136–139.

(21) Hodges, J. A.; Raines, R. T. Energetics of an $n \rightarrow \pi^*$ interaction that impacts protein structure. *Org. Lett.* **2006**, *8,* 4695–4697.

(22) Choudhary, A.; Gandla, D.; Krow, G. R.; Raines, R. T. Nature of amide carbonyl-carbonyl interactions in proteins. *J. Am. Chem. Soc.* **2009**, *131,* 7244–7246.

(23) Choudhary, A.; Kamer, K. J.; Powner, M. W.; Sutherland, J. D.; Raines, R. T. A stereoelectronic effect in prebiotic nucleotide synthesis. *ACS Chem. Biol.* **2010**, *5*, 655–657.

(24) Pollock, S. B.; Kent, S. B. H. An investigation into the origin of the dramatically reduced reactivity of peptide-prolyl-thioesters in native chemical ligation. *Chem. Commun.* **2011**, *47*, 2342–2344.

(25) Choudhary, A.; Fry, C. G.; Kamer, K. J.; Raines, R. T. An $n \rightarrow \pi^*$ interaction reduces the electrophilicity of the acceptor carbonyl group. *Chem. Commun.* **2013**, *49*, 8166-8168.

(26) Frisch, M. J.; Trucks, G. W.; Schlegel, H. B.; Scuseria, G. E.; Robb, M. A.; Cheeseman, J. R.; Scalmani, G.; Barone, V.; Mennucci, B.; Petersson, G. A.; et al. Gaussian 09, revision D.01; Gaussian, Inc.: Wallingford CT, **2013**.

(27) Foster, P.; Weinhold, F. Natural hybrid orbitals. *J. Am. Chem. Soc*. **1980**, *102*, 7211–7218.

(28) Tomasi, J.; Mennucci, B.; Cammi, R. Quantum mechanical continuum solvation models. *Chem. Rev.* **2005**, *105*, 2999-3093.

(29) Wang, J.; Wolf, R. M.; Caldwell, J. W.; Kollman, P. A.; Case, D. A. Development and testing of a general amber force field. *J. Comput. Chem.* **2004**, *25*, 1157–1174.

(30) Bayly, C. I.; Cieplak, P.; Cornell, W. D.; Kollman, P. A. A well-behaved electrostatic potential based method using charge restraints for deriving atomic charges: The RESP Model. *J. Phys. Chem.* **1993**, *97*, 10269–10280.

(31) Case, D. A.; Ben-Shalom, I.Y.; Brozell, S. R.; Cerutti, D.S.; Cheatham, III, T.E.; Cruzeiro, V.W.D.; Darden, T. A.; Duke, R. E.; Ghoreishi, D.; Gilson, M.K.; Gohlke, H.; Goetz, A.W.; Greene, D.;

Harris, R.; Homeyer, N.; et al. AMBER 2018, University of California, San Francisco, 2018.

(32) Jorgensen, W. L.; Chandrasekhar, J.; Madura, J. D.; Impey, R. W.; Klein, M. L. *J. Chem. Phys*. **1983**, *79*, 926.

(33) Chhabra, S. R.; Stead, P.; Bainton, N. J.; Salmond, G. P.; Stewart, G. S.; Williams, P.; Bycroft, B. W. Autoregulation of carbapenem biosynthesis in *Erwinia carotovora* by analogues of N-(3-oxohexanoyl)-L-homoserine lactone. *J. Antibiot.* **2003**, *46*, 441–454.

(34) Mattmann, M. E.; Blackwell, H. E. Small molecules that modulate quorum sensing and control virulence in *Pseudomonas aeruginosa*. *J. Org. Chem.* **2010**, *75,* 6737–6746.

(35) Eibergen, N. R.; Moore, J. D.; Mattmann, M. E.; Blackwell, H. E. Potent and selective modulation of the RhlR quorum sensing receptor by using non-native ligands: An emerging target for virulence control in *Pseudomonas aeruginosa*. *ChemBioChem,* **2015**, *16*, 2348–2356.

(36) Mattmann, M. E.; Shipway, P. M.; Heth, N. J.; Blackwell, H. E. Potent and selective synthetic modulators of a quorum sensing repressor in *Pseudomonas aeruginosa* identified from second-generation libraries of *N*-acylated-L-homoserine lactones. *ChemBioChem,* **2011**, *12*, 942–949.

(37) Choudhary, A.; Fry, C. G.; Raines, R. T. Modulation of an n→π* interaction with α-fluoro groups. *ARKIVOC,* **2010**, 251–262.

(38) Syrpas, M.; Ruysbergh, E.; Stevens, C. V.; De Kimpe, N.; Mangelinckx, S. Synthesis and biological evaluation of novel *N*-α-haloacylated homoserine lactones as quorum sensing modulators. *Beilstein J. Org. Chem.* **2014**, *10,* 2539–2549.

(39) Peterson, P. W.; Shevchenko, N.; Alabugin, I. V. "Stereoelectronic umpolung": Converting a p-donor into a σ-acceptor via electron injection and a conformational change. *Org. Lett.* **2013**, *9*, 2238 – 2241.

(40) Schneider, H. J.; Hoppen, V. Carbon-13 nuclear magnetic resonance substituent-induced shieldings and conformational equilibriums in cyclohexanes. *J. Org. Chem.* **1978**, *43*, 3866–3873.

(41) Hansch, C.; Leo, A.; Taft, R. W. A survey of Hammett substituent constants and resonance and field parameters. *Chem. Rev.* **1991**, *91*, 165–195.

(42) Pérez-Prior, M. T.; Manso, J. A.; del Pilar García-Santos, M.; Calle, E.; Casado, J. Reactivity of lactones and GHB formation. *J. Org. Chem.* **2005**, *70*, 420–426.

(43) Whiteley, M.; Diggle, S. P.; Greenberg, E. P. Progress in and promise of bacterial quorum sensing research. *Nat. Rev.* **2017**, *551*, 313–320.

TOC Image: